Inorg. Chem. **2008**, *47*, 10366−10371

Synthesis and Electrochemical Reaction with Lithium of Mesoporous Iron Oxalate Nanoribbons

María José Aragón, Bernardo León, Carlos Pérez Vicente, and José L. Tirado*

Laboratorio de Química Inorgánica, Universidad de Córdoba, Edificio C3, Campus de Rabanales, 14071 Córdoba, Spain

Received May 16, 2008

Mesoporous FeC_2O_4 was prepared by dehydration of bulk monoclinic- and micellar orthorhombic $FeC_2O_4 \cdot 2H_2O$ precursors at 200 °C. The micellar material shows nanoribbon shaped particles, which are preserved after dehydration. These solids are used as high-capacity lithium storage materials with improved rate performance. The mesoporous nanoribbons exhibit higher capacities close to 700 mA h/g after 50 cycles at 2C (C = 1 Li h^{-1} mol^{-1}) rate between 0 and 2 V.

Introduction

In recent years, nanomaterials have burst upon the scene of lithium battery research. New electrode materials have been recently found which provide higher capacities at higher rates by using the advantage of dispersion at the nanoscale and the enhanced stability of one-dimensional nanoparticles.[1−3] In parallel, a significant advance in the understanding of conversion electrode materials for lithium batteries has taken place. Transition metal oxides[3−6] and, more recently, transition metal fluorides[7,8] are known examples of solids involved in conversion reactions versus lithium. The electrochemical conversion process leads to the reduction of the metal ions to the metallic state together with the formation of lithium oxide or lithium fluoride, respectively. The partial reversibility of these processes makes these solids potential candidates for the negative or positive electrode of advanced lithium-ion batteries, respectively.

Recently, we were able to extend this process to submicrometric particles of manganese carbonate with the calcite structure.[9] This study revealed that $MnCO_3$ can be used directly as a conversion electrode versus lithium. The discharge of lithium test cells takes place by a different conversion reaction than that observed for the oxide produced during the thermal decomposition of the carbonate, MnO. Similar values of reversible capacity and better capacity retention were observed for the carbonate as compared with the oxide.

In this work, the study of oxysalts as conversion electrode material is investigated for a common and inexpensive compound: iron oxalate prepared by a novel synthesis procedure. The use of dehydrated nanoparticles of this compound provides interesting values of capacity at high rates.

Experimental Section

Two samples of iron(II) oxalate dihydrate were studied. Commercial iron oxalate (Panreac, Barcelona) was used as received. The synthesis of $FeC_2O_4 \cdot 2H_2O$ nanoparticles was carried out by a reverse micelles procedure from water-in-oil microemulsions. First, two microemulsions (I and II) were obtained under an argon atmosphere as follows. Microemulsion I contained cetyl-trimethylammonium bromide (CTAB) as the surfactant, hexanol as the cosurfactant, isooctane as the hydrocarbon phase and 0.3 M iron(II) sulfate solution as the aqueous phase. Microemulsion II has the same constituents as above except for having 0.3 M ammonium oxalate instead of iron sulfate as the aqueous phase. The weight

* To whom correspondence should be addressed. E-mail: iq1ticoj@uco.es.

(1) Armstrong, A. R.; Armstrong, G.; Canales, J.; García, R.; Bruce, P. G. *Adv. Mater.* **2005**, *17*, 862–865.
(2) Chan, C. K.; Peng, H.; Liu, G.; McIlwrath, K.; Zhang, X. F.; Huggins, R. A.; Cui, Y. *Nature Nanotech.* **2008**, *3*, 31–35.
(3) Li, Y.; Tan, B.; Wu, Y. *Nano Lett.* **2008**, *8*, 265–270.
(4) Poizot, P.; Laruelle, S.; Grugeon, S.; Tarascon, J. M. *J. Electrochem. Soc.* **2002**, *149*, A1212−A1219.
(5) Alcántara, R.; Jaraba, M.; Lavela, P.; Tirado, J. L. *Chem. Mater.* **2002**, *14*, 2847–2848.
(6) Lavela, P.; Otiz, G.; Tirado, J. L.; Zhecheva, E.; Stoyanova, R.; Ivanova, S. *J. Phys. Chem. C* **2007**, *111*, 14238–14246.
(7) Badway, F.; Mansour, A. N.; Pereira, N.; Al-Sharab, J. F.; Cosandey, F.; Plitz, I.; Amatucci, G. G. *Chem. Mater.* **2007**, *19*, 4129–4141.
(8) Liao, P.; MacDonald, B. L.; Dunlap, R. A.; Dahn, J. R. *Chem. Mater.* **2008**, *20*, 454–461.
(9) Aragón, M. J.; Pérez-Vicente, C.; Tirado, J. L. *Electrochem. Commun.* **2007**, *9*, 1744–1748.

10.1021/ic8008927 CCC: $40.75
Published on Web 10/11/2008

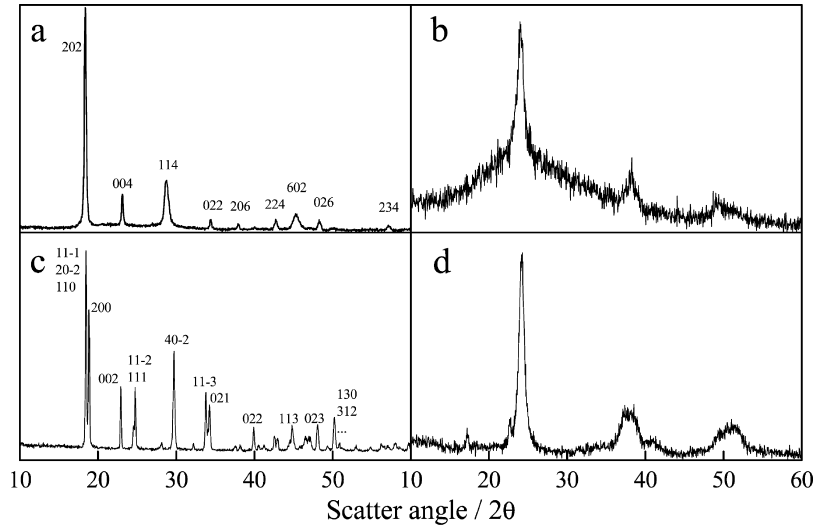

Figure 1. XRD patterns of iron oxalate samples: (a) micellar $FeC_2O_4 \cdot 2H_2O$, Miller indices for orthorhombic *Cccm*, (b) dehydrated (200 °C), FeC_2O_4 product from the micellar sample, (c) commercial $FeC_2O_4 \cdot 2H_2O$, Miller indices for *C*2/*m*, and (d) dehydrated (200 °C), FeC_2O_4 product from the commercial sample.

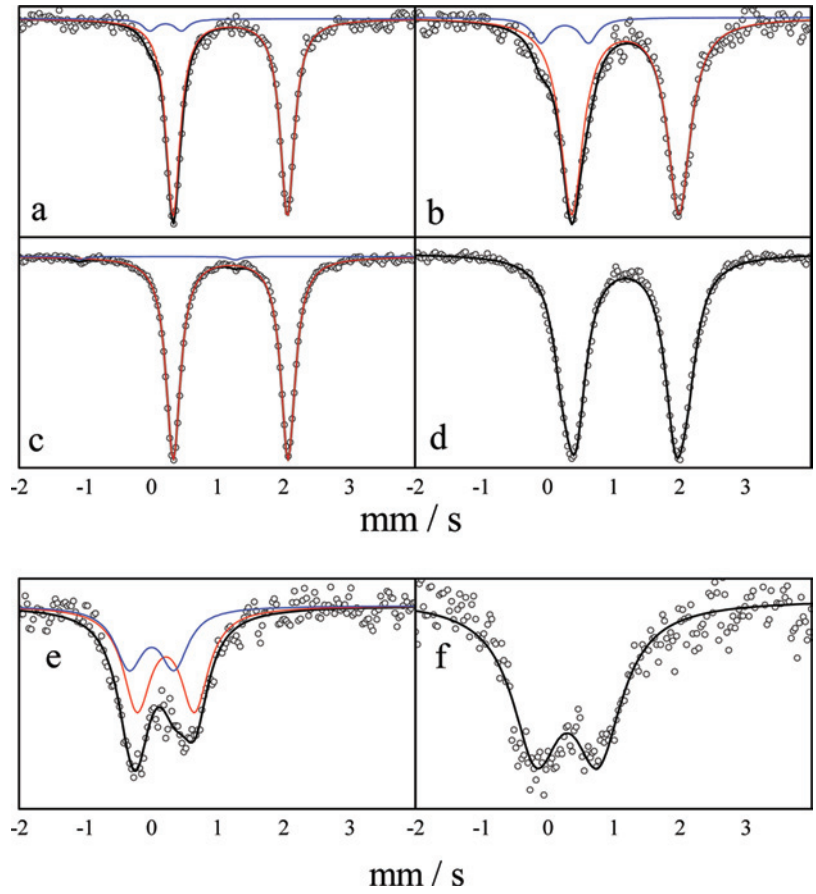

Figure 2. ^{57}Fe Mössbauer spectra of iron oxalate samples: (a) micellar $FeC_2O_4 \cdot 2H_2O$, (b) dehydrated FeC_2O_4 from micellar sample, (c) commercial $FeC_2O_4 \cdot 2H_2O$ (d) dehydrated FeC_2O_4 from commercial sample, (e, f) used electrodes after first discharge at 0 V and recharge at 3 V, respectively.

fractions of the various constituents in these microemulsions are as follows: 16.76% of CTAB, 13.9% of hexanol, 59.29% of isooctane, and 10.05% of the aqueous phase. In a second step, both microemulsions were slowly mixed and stirred overnight on a magnetic stirrer. The resulting precipitate was separated from the apolar solvent and surfactant by centrifugation followed by rinsing with a 1:1 mixture of methanol and chloroform. The different iron oxalate particles were subjected to a careful thermal decomposition at 200 °C under vacuum to yield anhydrous FeC_2O_4 nanoparticles.

X-ray diffraction (XRD) patterns were recorded on a Siemens D5000, using Cu Kα radiation and a graphite monochromator. ^{57}Fe Mössbauer spectra were recorded under the classical constant acceleration working mode using a conventional spectrometer. The source was 57Co(Rh). The velocity scale was calibrated using the sextet of a high-purity iron foil. All spectra were recorded at room temperature. Spectra were fitted to Lorentzian profiles by the least-squares method. Scanning electron microscopy (SEM) and transmission electron microscopy (TEM) images were obtained in a

Table 1. Fitting Results of the Mössbauer Spectra in Figure 2[a]

sample	IS	QS	LW	%	X^2
commercial	1.201_1	1.737_6	0.265_2	99_1	0.683
	0.09_2			1_1	
micellar	1.194_2	1.727_6	0.257_5	95_2	0.550
	0.22_3	0.48_5	0.26_9	6_5	
commercial 200 °C	1.182_7	1.63_1	0.386_7	100_1	0.935
micellar 200 °C	1.181_4	1.621_8	0.414_{10}	91_3	0.618
	0.26_3	0.72_4	0.32_6	9_7	
0.0 V	0.22_3	0.87_3	0.51_4	63_3	0.546
	0.00_4	0.68_6	0.5_1	36_7	
3.0 V	0.29_2	0.94_3	0.88_5	100_9	0.571

[a] IS, Isomer shift; QS, quadrupole splitting; LW, line width in mm/s.

JEOL JSM63000 microscope and JEOL 200CX microscope, respectively. Thermogravimetric (TG) and differential thermal analysis (DTA) curves were obtained in a SHIMADZU DTG-60AH instrument. N_2 adsorption isotherms at 77 K were obtained with a Quantachrome instrument.

For electrochemical tests, two-electrode Swagelok-type lithium test cells were used. The electrodes were prepared by blending the powdered active material (60%) with carbon black (30%) and poly vinylidene fluoride (10%) dissolved in N-methyl-pyrrolidone. The slurry was cast onto a Cu foil and vaccuum-dried at 120 °C. As the negative electrode, a lithium foil was used. The electrolyte was a solution of ethylene carbonate-diethyl carbonate in 1:1 weight proportion, including 1 M $LiPF_6$, supported by a porous glass-paper disk. The cells were assembled in an Ar-filled glovebox (H_2O, O_2 < 1 ppm). Galvanostatic charge/discharge cycles were carried out at 2C and 5C rates (C = 1 Li h^{-1} mol^{-1}).

Results and Discussion

According to early literature, $FeC_2O_4 \cdot 2H_2O$ crystallizes in two allotropic forms, α monoclinic *C*2/*c* and *β* orthorhombic *Cccm*.[10,11] The two samples studied in this work showed significant differences in their XRD data (Figure 1). Commercial iron oxalate showed a complex XRD pattern that could be interpreted in terms of a high-purity α form, with $a = 12.023_1$ Å, $b = 5.5550_6$ Å, $c = 9.913_1$ Å and $\beta = 128.563_5°$, in good agreement with Sledzinska et al.[11] In contrast, nanocrystalline synthetic oxalate showed the reflections ascribable to the orthorhombic *β* phase with $a = 12.290_5$ Å, $b = 5.542_3$ Å and $c = 15.460_4$ Å, also in good agreement with literature values.[10]

^{57}Fe Mössbauer spectra (Figure 2) were congruent with the data reported in the literature. For the monoclinic sample, a single quadrupole split signal was mainly observed with isomer shift IS = 1.201_1 mm/s and quadrupole splitting QS = 1.737_6 mm/s (Table 1), which is characteristic of Fe^{2+} ions in an environment with electric field gradient. Because of the existing dispersion of the Mössbauer data reported in the literature for this compound, the data obtained in this study agree with several previous reports but contrasts with the results in others.[12−15] In any case, the results are consistent with the structure description given to the monoclinic solid as infinite chains of the ferrous-oxalate ions linked together by hydrogen bonds engaging the oxygen atoms from the water molecules and the oxygen atoms belonging to the oxalate ions.[11] The Mössbauer spectra of the orthorhombic, micellar sample shows similar parameters for the main phase, apart from a slightly larger impurity content (ca. 6%), with IS = 0.22_3 mm/s closer to Fe^{3+} resulting from unavoidable oxidation during the synthesis in aqueous medium. The absence of marked differences in quadrupole splitting between the iron (II) oxalate dihydrate samples with a α- or *β*-structure is in agreement with an ionic structure. In oxalates of divalent metals, the covalency of the metal−oxygen bond is dependent on the electronegativity of the metal.[16] As compared with other divalent first-row transition metal ions, Fe^{2+} has a higher ionicity, and the main contribution to the

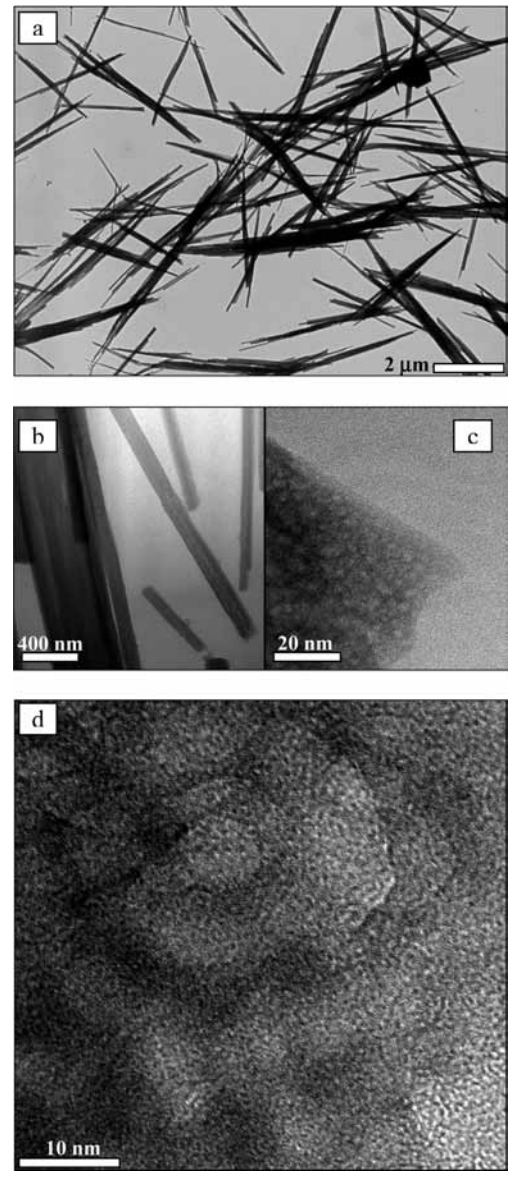

Figure 3. TEM images of (a) micellar raw material, and (b−d) after thermal decomposition at 200 °C under vacuum.

(10) Deyrieux, R.; Peneloux, A. *Bull. Soc. Chim. Fr.* **1969**, *8*, 2675–2681.
(11) Sledzinska, I.; Murasik, A.; Piotrowski, M. *Physica* **1986**, *138B*, 315–322.
(12) Brady, P. R.; Duncan, J. F. *J. Chem. Soc.* **1964**, 653–656.
(13) Gabal, M. A.; El-Bellihia, A. A.; Ata-Allah, S. S. *Mater. Chem. Phys.* **2003**, *81*, 84–92.
(14) Takashima, Y.; Tateishi, Y. *Bull. Chem. Soc. Jpn.* **1965**, *38*, 1688–1693.
(15) Ravi, N.; Jagannathan, R. *Hyperfine Interact.* **1982**, *12*, 167–173.
(16) Devillers, M.; Ladrière, J.; Apers, D. *Inorg. Chim. Acta* **1987**, *126*, 71–77.

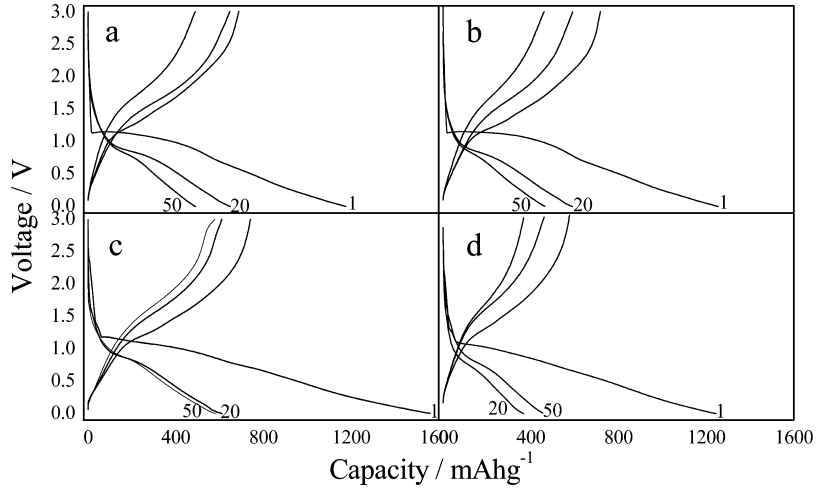

Figure 4. Cycling experiments at (a, c) 2C and (b, d) 5C for micellar (c, d) and commercial (a, b) dehydrated samples.

quadrupole splitting comes from the electronic configuration; thus, the lattice contribution can be neglected.[16,17]

The two oxalate samples crystallized with two water molecules. Thermogravimetric curves were recorded to locate the temperature at which the two water molecules are released from $FeC_2O_4 \cdot 2H_2O$. The observed weight loss up to 200 °C (20.1% for the commercial sample and 21.2% for the micellar sample) agrees perfectly with the theoretical value (20.02%). At temperatures larger than 200 °C, a second weight loss effect is visible in the TG curves, which is ascribable to oxalate decomposition to magnetite.[18] Irrespective of the origin of the oxalate sample and the crystallographic structure of the starting solid, the XRD patterns of the dehydrated products (Figure 1b,d) showed a small number of highly broadened reflections which agreed well with a poorly crystalline solid with a FeC_2O_4 composition.[18]

The dehydrated product resulting from the commercial sample consisted of particles of several micrometers with heterogeneous particle size and shape. TEM micrographs of the dehydrated micellar oxalate showed ultrafine particles (Figure 3) with elongated shapes. Nanoribbons about 150 nm wide are observed for the sample obtained using reverse micelles. Both samples dehydrated at 200 °C showed a complex porous texture (see, for example, Figure 3d) with pores probably created during water release. This observation is consistent with the Brunauer−Emmett−Teller (BET) surface values obtained from the N_2 adsorption isotherms (ca. 70 $m^2\ g^{-1}$ for both samples). The mesoporous material is then obtained by a top-down approach, which has been recently found in conversion electrodes.[19]

The Mössbauer spectra of the dehydrated samples (Figure 2b,d) evidence a highly broadened signal that could be fitted to multiple quadrupole split doublets, indicative of multiple closely related environments of iron atoms. This behavior can be explained by assuming ultrafine particles in which surface iron atoms are affected by a larger electric field gradient than inner atoms. The average IS and QS values are collected in Table 1, which are also indicative of little changes in the oxidation state of iron during the dehydration reaction.

The electrochemical reaction of FeC_2O_4 with lithium took place with a first extended plateau (ca. 1200 mA h g^{-1} at 5C rate) at about 1 V versus Li (Figure 4) leading to an X-ray amorphous product. As commonly found in conversion electrodes,[1] the initial irreversible capacity is large. Further cycles displayed up to 750 mA h g^{-1} reversible capacities, which doubles the theoretical capacity of graphite (372 mA h g^{-1}).

To gain further insight on the electrochemical reaction that takes place in these electrode materials, the first step was to examine the nature of the reduced products by an iron-selective spectroscopy. The ^{57}Fe Mössbauer spectroscopy study of used electrodes was carried out by interrupting the cycling experiments at selected voltages. The spectrum at 0 V (Figure 2e) shows a complex profile in which both the average isomer shift and QS approaches to that α-iron. However the value is above 0 mm/s, which agrees with a noncrystalline phase, observed by XRD. Thus these results can be interpreted as the result of iron reduction to the metallic state in the form of metal nanoparticles in contact with $Li_2C_2O_4$. The iron particles show superparamagnetic behavior. In an attempt to fit the observed spectra to a simplified model, two doublet signals were obtained (Table 1). As referred to recent reports on iron oxides,[20,21] these doublets could account for two different environments of partly reduced iron: surface iron (with higher IS and QS) and bulk metallic atoms (with hyperfine parameters closer to those of α-Fe). The contribution of the former is expected to grow markedly on decreasing particle size. The percentage of surface atoms in regular octahedral nanoparticles could be close to 63% for particles containing few hundreds of atoms.

(17) Aramu, F.; Maxia, V.; Muntoni, C. *Lett. Nuovo Cimento* **1975**, *12*, 225–227.
(18) Brown, R. A.; Bevant, S. C. *J. Inorg. Nucl. Chem.* **1966**, *28*, 387–391.
(19) Hu, Y. S.; Guo, Y. G.; Sigle, W.; Hore, S.; Balaya, P.; Maier, J. *Nat. Mater.* **2006**, *5*, 713–717.
(20) Alcántara, R.; Jaraba, M.; Lavela, P.; Tirado, J. L.; Jumas, J. C.; Olivier-Fourcade, J. *Electrochem. Commun.* **2003**, *5*, 16–21.
(21) Bomio, M.; Lavela, P.; Tirado, J. L. *ChemPhysChem* **2007**, *8*, 1999–2007.

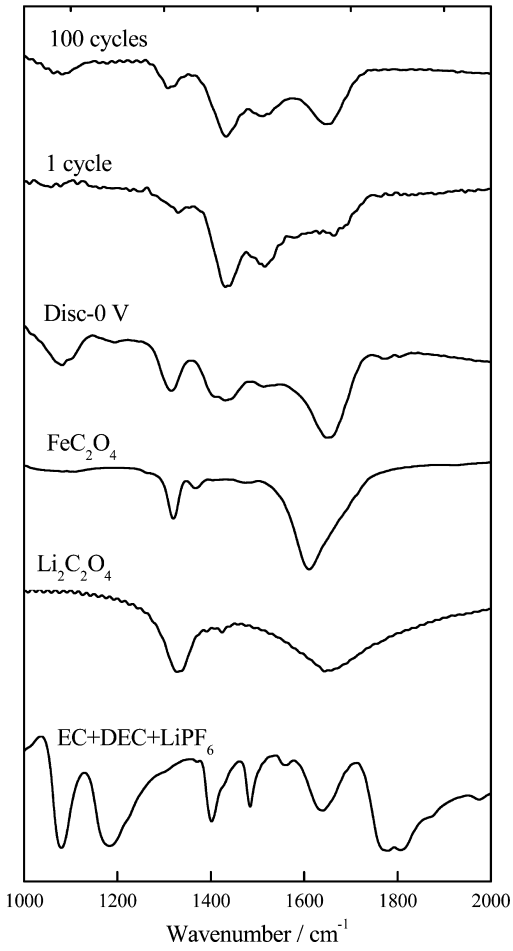

Figure 5. FTIR spectra of electrolyte, FeC_2O_4, $Li_2C_2O_4$, and charged and discharged electrodes.

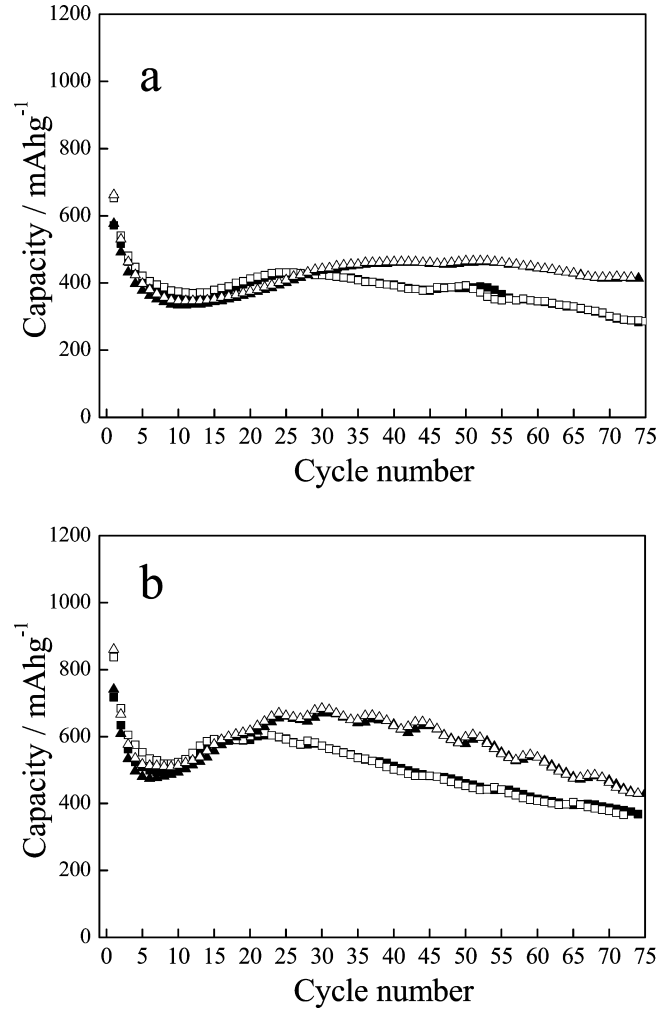

Figure 6. Cycling experiments at (a) 5C and (b) 2C for micellar (triangles) and commercial (circles) dehydrated samples. Disharge (empty symbols) and charge (filled) capacities are shown.

After cell discharge to 0 V followed by a charge process to 3 V, the MS of the pristine sample is not recovered (Figure 2f). Instead, a highly broadened spectrum resulting from multiple doublets is visible, with average IS and QS values close those expected for Fe^{3+} ions. The ultrafine nature of the oxidized domains prevents again a ferromagnetic ordering. The origin of the complex signal with different QS but differing less that in the case of the metal nanoparticles may be a consequence of a different spin state of the atoms in the structure of the oxalate nanoparticles.

Additional experiments were performed to check the integrity of oxalate ions in the used electrodes. FTIR data (Figure 5) confirms that oxalate ions are preserved on cycling. Particularly, the band at about 1320 cm^{-1}, which is characteristic of both FeC_2O_4 and $Li_2C_2O_4$, is absent in the electrolyte and visible in charged and discharged electrodes. Thus, it can be concluded that the system is significantly different from conventional conversion oxide electrodes, as the matrix formed during the discharge is lithium oxalate instead of lithium oxide.

To deepen in the possible formation of FeC_2O_4 or FeO on charge, the information obtained in this study by looking at the recharged electrodes, XRD, MS, and FTIR, is summarized as follows. The results unequivocally show that the original iron(II) oxalate is not recovered after charge and that no iron(II) oxide is formed. First, the product was X-ray amorphous. Second, the MS spectrum (Figure 2f and Table 1) shows a doublet signal with an IS value (0.29 mm/s) which is intermediate between that of Fe(0) and that of Fe(III). Fe(II) is well-known to occur in the 1.00−1.50 mm/s IS range in oxides and carboxylates.[22,14] The QS value also differs from the original oxalate (Figure 2b,d). In consequence, the presence of Fe(II) compounds such as FeO or FeC_2O_4 can be discarded in the cycled electrode. Finally, the FTIR data obtained in transmission mode (Figure 5) support the presence of oxalate counterions in a partly oxidized amorphous product different from the conventional oxide products reported by other authors in conversion oxide electrodes. The initial oxalate ions are not decomposed during the charge−discharge processes, as shown by the absence of gaseous products that could have caused overpressure and/or breakage in the test cells.

The electrochemical behavior in lithium test cells of $FeC_2O_4 \cdot 2H_2O$ polycrystalline samples in both allotropic forms was poor. In contrast, the cyclability of both dehydrated oxysalts was significantly improved. The results for both FeC_2O_4 samples are compared in Figure 6. Even cycling

(22) Smith, M. G.; Goodenough, J. B. *J. Solid State Chem.* **1993**, *103*, 25–29.

at higher rate, iron oxalate shows higher capacity than the previously reported manganese carbonate.[9] Capacities are always above 600 mA h g^{-1} during 75 cycles when iron oxalate is cycled at 2C rate.

In conclusion, first-row transition metal oxysalts are interesting candidates for the active material of the negative electrode of lithium-ion batteries. The low temperature synthesis of these materials makes them an inexpensive option for this purpose.

Acknowledgment. The authors are indebted to MEC (MAT2005-00374) and Junta de Andalucía (FQM288).

IC8008927